Available online at www.sciencedirect.com
ScienceDirect
Acta Materialia 56 (2008) 5751–5763
Acta MATERIALIA
www.elsevier.com/locate/actamat

Mechanisms and kinetics of MgB_2 synthesis from boron fibers

John D. DeFouw *, David C. Dunand

Department of Materials Science and Engineering, Northwestern University, 2220 Campus Dr, Evanston, IL 60208, USA

Received 12 March 2008; accepted 22 July 2008
Available online 1 September 2008

Abstract

Superconducting MgB_2 fibers were synthesized through the reaction of liquid magnesium with 140 μm diameter boron fibers. Fiber reaction occurs by two concurrent mechanisms. First, concentric MgB_2, MgB_4 and MgB_7 shells grow radially into the B fibers. Diffusion modeling provides rate constants and effective diffusion coefficients for the borides and their activation energies. Second, radial cracks form in the MgB_4 or MgB_7 shells, allowing for Mg ingress into the fibers and diffusional growth of MgB_2 wedges in the radial and circumferential directions. Combining both shell and wedge MgB_2 growth mechanisms into a single model provides predictions of overall MgB_2 reaction kinetics as a function of time and temperature, which are in good agreement with in situ X-ray diffraction measurements performed at 885–1025 °C.

Keywords: Theory and modeling (kinetics, transport, diffusion); Chemical synthesis; X-ray diffraction; Superconductor; Magnesium diboride

1. Introduction

Superconducting MgB_2 can be synthesized from elements via the reaction:

$$Mg + 2B = MgB_2 \quad (1)$$

The kinetics of this reaction have been studied for elemental powders [1–4], as they are relevant to the fabrication of MgB_2 wires by the powder-in-tube method [5–9]. We recently studied, for commercial submicrometer B powders, the times to achieve complete reaction, e.g. 10 min at 900 °C and 2 h at 700 °C for 400 nm B powder agglomerates [2]. Kinetics results were fitted to diffusion-based models, from which diffusion coefficients between 3×10^{-16} and 2×10^{-17} $m^2 s^{-1}$ and activation energies between 123 and 143 kJ mol^{-1} were calculated [2]. However, the complex shape of the 400 nm powder agglomerates, consisting of loosely connected 10–50 nm spheroidal particles, and the presence of intermediate magnesium borides (MgB_{20}, MgB_7, MgB_4) complicate the determination of kinetic parameters.

Continuous MgB_2 fibers can be synthesized by reacting commercial boron fibers with Mg vapor [10] or liquid Mg [11]. As compared to the above agglomerates of 10–50 nm B particles [2], these B fibers are much larger (100–200 μm in diameter) and they have much simpler geometries, making modeling more accurate: they are dense, highly pure (99.999%) and nearly perfectly cylindrical in shape [12]. The reaction of such commercial B fibers into MgB_2 fibers has been shown to be completed in 2 h at 950 °C through exposure to Mg in the gas [10] or liquid [11] phase. Reaction with liquid Mg is accompanied by cracking of the MgB_2 fibers, as a result of the volume increase associated with the synthesis (Eq. (1)), leading to radial cracks that do not connect with each other and thus do not lead to disintegration of the fibers [11]. If excess liquid Mg is used, it can be solidified after completion of the reaction to form a Mg matrix surrounding these straight, continuous, superconducting MgB_2 fibers [11].

In the present paper, the reaction kinetics for the synthesis of MgB_2 fibers from commercial B fibers in liquid Mg (Eq. (1)) are investigated over a broad range of temperatures (700–1025 °C) and modeled to determine kinetic parameters such as rate constants, diffusion coefficients and activation energy. The effect of cracking associated

* Corresponding author. Tel.: +1 847 467 3996.
E-mail address: jdefouw@u.northwestern.edu (J.D. DeFouw).

1359-6454/$34.00 © 2008 Acta Materialia Inc. Published by Elsevier Ltd. All rights reserved.
doi:10.1016/j.actamat.2008.07.049

with the B → MgB_2 volume increase is also incorporated in these models.

2. Materials and methods

Commercial B fibers with 99.999% purity and 140 μm diameter (from Specialty Materials, Inc., Lowell, MA) were cut to 20 mm long segments and aligned in a 100 mm long pure titanium crucible with 8 and 9.5 mm inner and outer diameters. The evacuated fiber preform was then pressure-infiltrated with liquid Mg at 800 °C [11,13] and immediately cooled to prevent reaction between Mg and B. The crucible containing the solidified Mg–B composite was transferred to the beamline end station 5-BM-D (DuPont-Northwestern-Dow Collaborative Access Team Synchrotron Research Center) at the Advanced Photon Source (Argonne National Laboratory, IL) for diffraction experiments using a 65 keV ($\lambda = 0.019$ nm) synchrotron X-ray beam with a square 1 mm^2 cross-section. A radiant furnace heated the sealed crucible through the evacuated quartz tube to 500 °C in 5 min. After a 5 min hold to equilibrate temperature, the quartz tube was back-filled with 0.33 atm of argon (a pressure maintained constant during the experiment to prevent bulging of the crucible subjected to the vapor pressure of Mg) and the crucible was heated in 5 min to the reaction temperature chosen in the range 885–1025 °C (i.e. above the 650 °C melting point of Mg). No significant reaction was detected by diffraction before reaching the desired reaction temperature.

Transmitted diffraction rings were recorded, after 30–120 s exposures times, on a 150 mm diameter charge-coupled device camera (Photonic Science Limited, UK) placed ~380 mm from the sample. The ring intensities were first integrated over their circumferences to create plots of intensity versus 2θ (where θ is the diffraction angle), using FIT2D software [14]. The intensity of the $(10\bar{1}1)$ MgB_2 peak (after background subtraction and integration over a typical 2θ range of 4.9–5.2° using JADE 6.5 powder diffraction software) was then determined for each diffraction pattern. This intensity was divided by the peak intensity after full reaction to provide the degree of reaction, which is equivalent to the fraction of consumed B (or alternatively to the fraction of synthesized MgB_2) defined as the instantaneous B (respectively, MgB_2 synthesized) volume consumed divided by the original B volume (respectively, final MgB_2 volume after complete reaction). Peaks for MgB_4 and MgB_7 were not resolved due to a lack of diffraction intensity. Further details and a schematic of the experimental equipment are given in a previous publication [2], where similar experiments were performed on Mg and B powders.

The microstructure of reacted fibers was analyzed ex situ by quenching specimens, cutting the composite perpendicular to the fiber axis, and preparing metallographic cross-sections. The thicknesses of the shells of reaction products (MgB_2, MgB_4 and MgB_7) surrounding the partially reacted B fibers were measured at five locations for each of ten fibers by optical microscopy after exposure times of 1–5 min at 1000 °C, 15–100 min at 900 °C, 1–5 days at 800 °C and 21–123 days at 700 °C.

3. Results

Fig. 1 shows the time dependence of the MgB_2 degree of reaction x as determined by in situ X-ray diffraction. Reaction curves are sigmoidal in shape, with a period of slow reaction for $x < 0.04$ (following an incubation time for the lowest temperature), a rapid increase in reaction rate up to $x \sim 0.8$ and a region of slowing reaction kinetics up to completion ($x = 1$). The time to achieve complete reaction increases from 1 to 10 h as temperatures decreases from 1025 to 885 °C.

As reported in other studies [15,16] and in accordance with the Mg–B phase diagram [17], three intermediate borides (MgB_{20}, MgB_7, MgB_4) should be present before the reaction reaches equilibrium, when MgB_2 is created according to Eq. (1) in the presence of excess Mg. Metallographic examination of partially reacted fibers at 900 and 1000 °C shows that three boride shells are growing into the B fiber, as illustrated in Fig. 2 for fibers reacted for 1–5 min at 1000 °C: a first outer MgB_2 shell with 4–8 μm thickness, a second MgB_4 layer with 9–40 μm thickness, and an inner 1–3 μm thick MgB_7 shell. A MgB_{20} shell is not observed, either because it is too thin to be visible or because of lack of compositional contrast with B. The three phases were identified by time-of-flight secondary ion mass spectrometry and are similar to other observations of partially reacted fibers [15]. It is apparent that the two inner MgB_7 and MgB_4 shells are growing at similar high rates, with about three-quarters of the B fiber volume converted to MgB_7/MgB_4 after only 5 min at 1000 °C (Fig. 2d). The outer MgB_2 shell is much slower, with ~15% of the B fiber

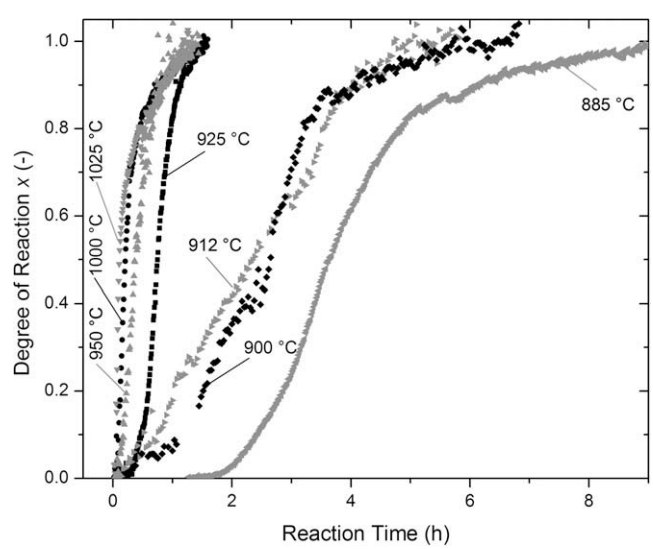

Fig. 1. Time dependence for MgB_2 degree of reaction measured by synchrotron X-ray diffraction for B fibers reacted in situ with liquid Mg.

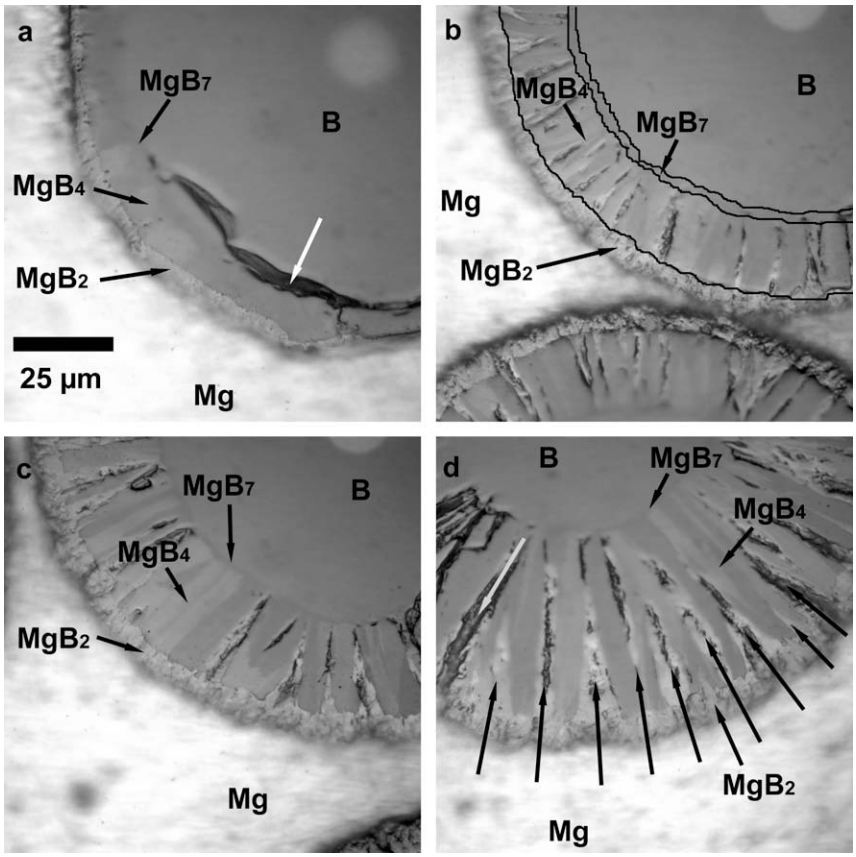

Fig. 2. Optical micrographs of B fibers partially reacted with liquid Mg at 1000 °C for (a) 1 min, (b) 2 min, (c) 3 min and (d) 5 min, showing concentric MgB_2, MgB_4 and MgB_7 shells surrounding an unreacted B core (phase boundaries are highlighted with black lines in (b)). The gray arrow in (d) indicates a radial crack in the MgB_2 and MgB_4 shells infiltrated by Mg, while the white arrow in (a) shows a circumferential crack not due to reaction but likely from metallographic preparation. Black arrows in (d) point to MgB_2 wedges (with some damage due to metallographic preparation) growing into the MgB_4 shell.

fully converted to MgB_2 after 5 min, and full conversion taking about 1 h, as measured by in situ diffraction (Fig. 1).

As illustrated in Fig. 2b–d, the intermediate MgB_4 shell contains radial cracks which span the whole width of the shell and are filled with MgB_2. Thus, MgB_2 synthesis occurs both by the growth of the outer cylindrical MgB_2 shell and by the conversion of MgB_4 at numerous radial cracks, resulting in MgB_2 wedges growing both in length and width. These cracks may in fact extend to the surface of the fiber allowing for the rapid ingress of Mg deep into the fiber, and sustaining the rapid growth of the associated MgB_2 wedge. Indeed, Fig. 2d illustrates that some of the

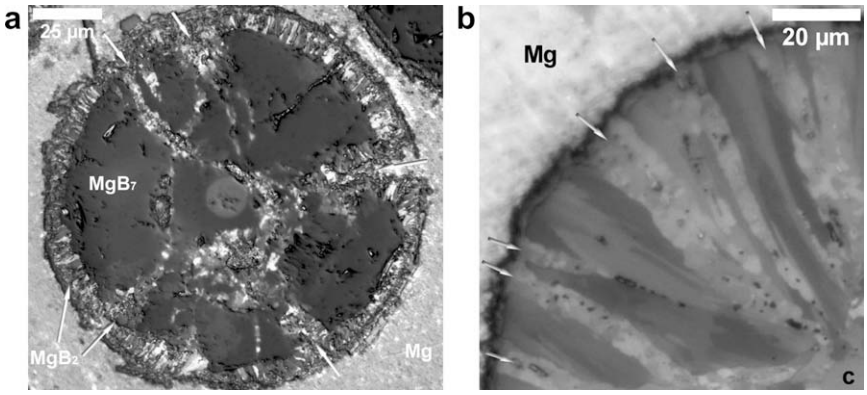

Fig. 3. Optical micrographs of B fibers partially reacted with liquid Mg (a) at 800 °C for 5 days (degree of reaction $x \sim 0.3$), showing irregular cracking within the MgB_7 phase associated with MgB_2 veins, together with a MgB_2 shell surrounding the fiber and (b) at 900 °C for 2 h ($x \sim 0.4$), showing a thin outer MgB_2 shell and thicker MgB_2 wedges (light grey regions indicated by arrows) growing radially towards the fiber W–B core (marked *c*), leaving MgB_4 slivers (medium and dark grey regions) throughout the fiber.

radial cracks contain elemental Mg. This short-circuit mechanism for MgB_2 growth effectively increases the surface of fibers reacting with Mg.

At lower temperatures (700 and 800 °C), optical micrographs show the MgB_2 shell grew from 3 to 10 μm over reaction times of 21–123 days at 700 °C and 1–5 days at 800 °C (Fig. 3a), but no MgB_4 shell was visible. Since this phase must be thermodynamically present, it is assumed to be very thin and not resolvable by optical microscopy. By contrast, at these lower temperatures, the MgB_7 shell grew from 25 to 70 μm (i.e. to the center of the fiber) over the same time periods, at a much faster rate than the MgB_2 (and putative MgB_4) shells. While cracks forming at 900 and 1000 °C in the MgB_2 shell are straight and radially oriented (Fig. 2b–d), those forming in the MgB_7 shell at lower temperatures are much less regular in shape and orientation, leading to MgB_2 veins as illustrated in Fig. 3a for a fiber reacted for 5 days at 800 °C.

Fig. 3b shows a B fiber for a sample having reached an average MgB_2 degree of reaction of ~40% (as measured optically) after 2 h at 900 °C. The MgB_2 wedges have reached the tungsten boride (W–B) core of the fiber, but multiple radial slivers of MgB_4 are visible. They correspond to the regions of the MgB_4 shell between the MgB_2 wedges, which convert slowly to MgB_2 by diffusion-controlled lateral (circumferential) growth of the MgB_2 wedges.

4. Discussion

4.1. Modeling of reaction rates

Because of the relatively rapid heating rate (1–2 °C s^{-1}) used in the present experiments, no MgB_2 was observed in diffraction patterns before the isothermal temperature was reached. The experimental data can thus be fitted to a model for the isothermal diffusion-limited reaction of cylin-

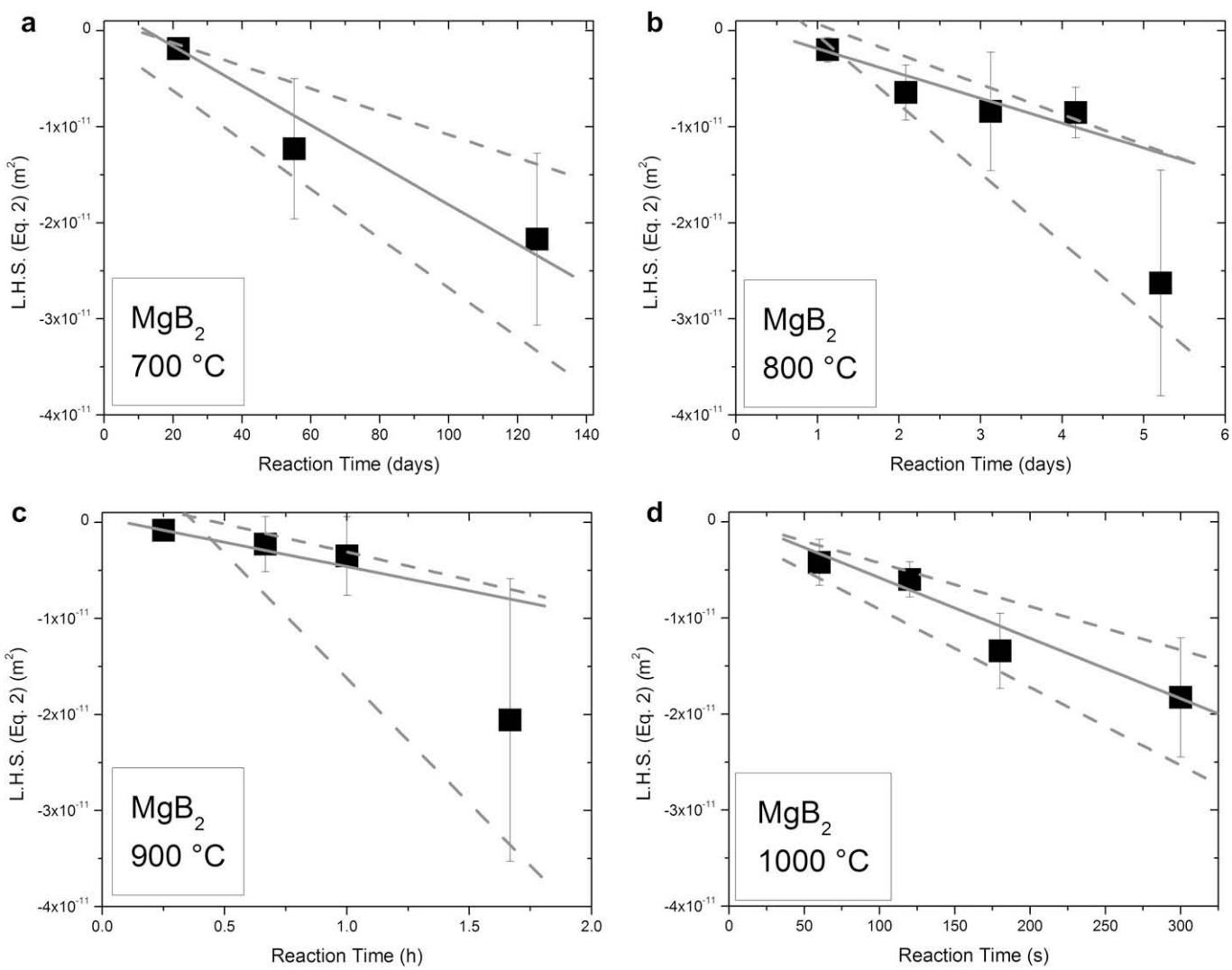

Fig. 4. Left-hand side of Eq. (2), calculated from ex situ measurements of MgB_2 shell thickness (e.g. Fig. 2), as a function of reaction time at 700–1000 °C. Reaction rates are slopes of solid line through data points, with the slopes of the dotted lines, calculated using the extreme of the error bars, providing the reaction rate errors.

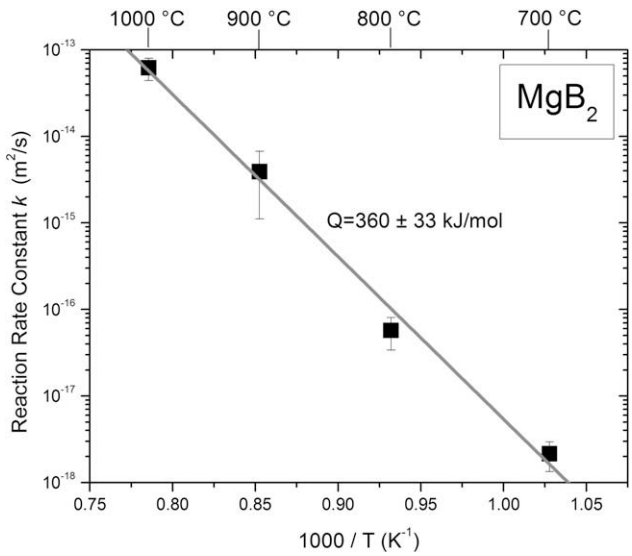

Fig. 5. Arrhenius plot of MgB_2 reaction rate constant k (as determined from Fig. 4) vs. inverse temperature, showing activation energy $Q = 360$ kJ mol^{-1}.

ders in a gas or liquid, derived in Appendix A based on an original derivation by Carter [18] for reacting spheres, which relates the degree of reaction x with the reaction time t as

$$\frac{r_0^2}{4(z-1)}\left(x\ln\left(\frac{1-x+zx}{1-x}\right)+zx\ln\left(\frac{1-x}{1-x+zx}\right)+z\ln\left(\frac{1}{1-x}\right)+\ln\left(\frac{1-x}{1-x+zx}\right)\right)=-kt, \quad (2)$$

where z is the volume expansion coefficient ($z = 1.90$ for the B → MgB_2 reaction [19]), r_0 is the initial fiber radius, and k is the reaction rate constant. Eq. (2) takes explicitly into account that the reaction occurs at a cylindrical interface with a volume change given by the parameter z, and is valid until completion ($x = 1$).

The MgB_2 shell thicknesses h measured from micrographs, as illustrated in Fig. 2a–d, were converted to degree of reaction x through Eq. (A8) in Appendix A. The degree of reaction was then used to calculate the left-hand side of Eq. (2), with errors propagated from the thickness measurements, which is plotted as a function of reaction time in Fig. 4a–d at 700–1000 °C. The slope of the best-fit lines through these plots is then, according to Eq. (2), the rate constant k for diffusional growth of MgB_2. These rate constants span values from 2×10^{-18} m^2 s^{-1} at 700 °C to 6×10^{-14} m^2 s^{-1} at 1000 °C. The rate constant at 800 °C is 6×10^{-17} m^2 s^{-1}, which is equal, within experimental error, to the rate constant of 5×10^{-17} m^2 s^{-1} determined from experiments where a thin B film was exposed to Mg vapor to form a MgB_2 layer at 800 °C [2,20].

An Arrhenius plot of the rate constants versus inverse temperature yields an activation energy of 360 kJ mol^{-1} for MgB_2 shell growth (Fig. 5). This activation energy is much larger than the range of values found for B powders (108–146 kJ mol^{-1}) in our previous study using synchrotron diffraction [2]. This discrepancy may be explained as follows. The present B fibers are dense, perfect cylinders immersed in liquid Mg, while the B powders were irregular agglomerates of nanometric particles that were not completely infiltrated with liquid Mg and thus probably reacted also with Mg vapor. Additionally, the reaction layer thickness in the present fibers was 3–10 μm, while the particle agglomerate radius was 0.2 μm, leading to a much smaller reaction layer than for the present fibers.

4.2. Modeling of diffusion coefficients

Entchev et al. [21] developed a model predicting the normalized shell thickness h^* (shell thickness divided by initial cylinder radius r_0) produced by a synthesis reaction, with numerical solutions for volume expansion $z = 1$ (reactant and product have same density) and $z = 1.77$ (relevant to the transformation of Ti into TiO_2). In the present case, we use a thickness h' (equal to $h^* r_0$ for $z = 1$ and corresponding to the thickness of consumed B), with the value of h^* plotted by Entchev et al. in Fig. 9 of Ref. [21] as a function of the dimensionless reaction time $t^* = Dt/r_o^2$, where D is the effective diffusion coefficient for the reaction. This plot was fitted to a fifth-degree polynomial equation, providing:

$$h' = r_0[A_5 t^{*5} + A_4 t^{*4} + A_3 t^{*3} + A_2 t^{*2} + A_1 t^* + A_0], \quad (3)$$

where $A_5 = 0.4092$, $A_4 = -2.095$, $A_3 = 4.004$, $A_2 = -3.527$, $A_1 = 1.795$ and $A_0 = 0$. Because multiple boride shells exist, the scaled thickness h'_i of the consumed B shell was calculated for each boride i by dividing the average boride shell thickness h_i, as measured by optical microscopy at locations away from cracks, with the parameter $z^{1/2}$ ($z = 1.90$ for MgB_2, 1.47 for MgB_4, and 1.18 for MgB_7 as calculated from density and molar volume [19]). The exponent 1/2 reflects that the reaction predominantly occurs in the two radial dimensions of the fibers, whose 20 mm length is much larger than its diameter (0.14 mm). The sum of the scaled thicknesses h'_i for each boride shells is then the scaled cumulative thickness h'. Plots of h' versus t, shown in Fig. 6a–c for a reaction temperature of 1000 °C, are fitted to Eq. (3), with the diffusion coefficient D as the fitting parameter. The resulting diffusion coefficients for each boride are shown in Arrhenius plots in Fig. 7, from which activation energies $Q = 362 \pm 41$, 477 ± 41 and 319 ± 25 kJ mol^{-1} are determined for MgB_2, MgB_4 and MgB_7, respectively. The diffusion coefficient for MgB_2 at 800 °C ($D = 6 \times 10^{-16}$ m^2 s^{-1}) is reasonably close, given experimental errors, to the value ($D = 1 \times 10^{-16}$ m^2 s^{-1}) found for a B thin film reacted in Mg vapor at 800 °C [20]. Also, the activation energy for the diffusion coefficient of MgB_2 ($Q = 362 \pm 41$ kJ mol^{-1}) is in agreement with the value ($Q = 360$ kJ mol^{-1}) found in the previous section for the reaction rate. However, it is much higher than the values ($Q = 123$–143 kJ mol^{-1}) determined in our previous study [2] for the diffusion coefficient in nanometric B powders, for the same reasons discussed in the previous section.

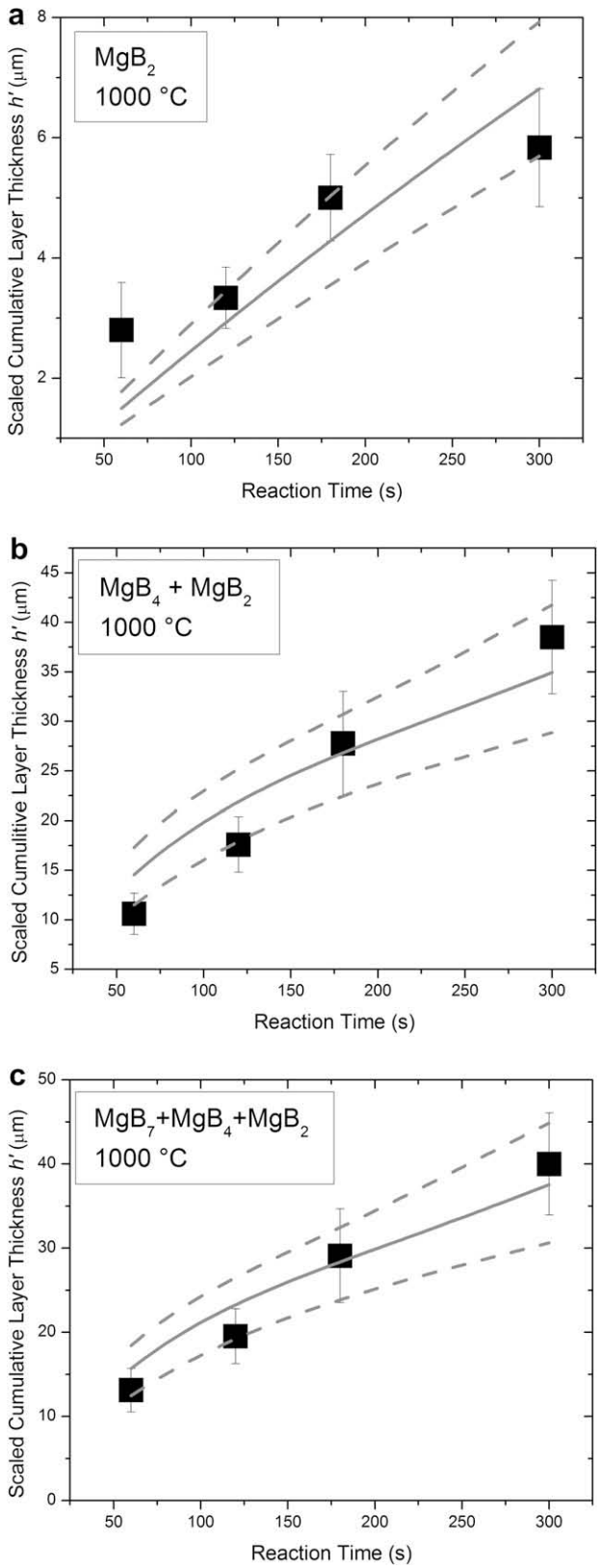

Fig. 6. Plots of scaled cumulative thickness of reaction shells vs. reaction time at 1000 °C for (a) MgB_2, (b) $MgB_2 + MgB_4$ and (c) $MgB_2 + MgB_4 + MgB_7$. Fits of data by Eq. (3) are shown as lines, with the diffusion coefficient as a fitting parameter. Dotted lines are fitted through the extreme of the error bars and provide errors for the diffusion coefficients.

4.3. Modeling of reaction with shell cracking

In the previous sections, only the boride shells formed outside the fiber are considered, from which the MgB_2 reaction rate and the MgB_2, MgB_4 and MgB_7 diffusion coefficients can be determined. To predict overall fiber reaction, it is necessary to take into account the cracks forming into the MgB_4 shell (or, at low temperature, the MgB_7 shell) due to the large volume expansion associated with the boride formation, which create a much larger area for the diffusion-controlled creation of MgB_2. The first and second steps of the reaction in Eq. (1), $B \rightarrow MgB_7$ and $MgB_7 \rightarrow MgB_4$, are associated with an 18 and 24% volume increase, respectively. The final $MgB_4 \rightarrow MgB_2$ conversion exhibits a 29% volume increase, leading to an overall volume change of 90% ($z = 1.90$) for the $B \rightarrow MgB_2$ reaction. Each of these volume changes produces strains that are much larger than can be sustained elastically by the boride phases, so cracks are expected to form, as observed experimentally in Fig. 2b–d, allowing liquid Mg to infiltrate and react to MgB_2 within the crack.

The chain of events is illustrated schematically in Fig. 8a–d. Very early (Fig. 8a), three concentric, cylindrical, crack-free shells of MgB_2, MgB_4 and MgB_7 form at the fiber surface and grow radially towards its center. Later (Fig. 8b), cracks form in the MgB_4 shell, allowing liquid Mg to infiltrate and react to MgB_2 wedges within the cracks. Alternatively, transport of Mg through filled cracks may occur without ingress of liquid Mg by interfacial diffusion at the interface of the MgB_2/MgB_4 wedge and/or by grain boundary diffusion, both of which are expected to be much more rapid than lattice diffusion. At later times

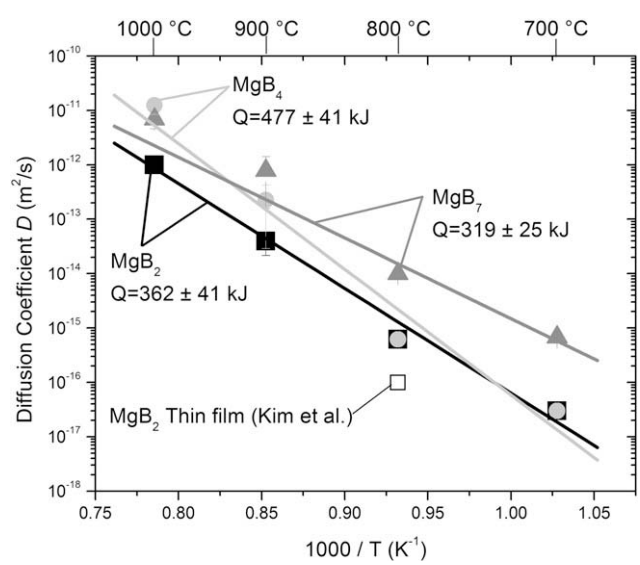

Fig. 7. Arrhenius plot of diffusion coefficients D vs. inverse temperature, where D is determined from Fig. 6 at 1000 °C (and similar plots at other temperatures) for the growth of MgB_2, MgB_4, and MgB_7 shells. Best-fit lines result in activation energies Q listed in the figure. Diffusion coefficient calculated for a B thin film reacted in Mg vapor at 800 °C [20] is also shown.

(Fig. 8c), MgB_2 growth continues on two reaction fronts with the MgB_4 phase, the first at the MgB_2/MgB_4 shell interface and the other at the MgB_2/MgB_4 wedge interfaces. The MgB_4 and MgB_7 shells continue to progress radially into the fiber. Near the end of the reaction (Fig. 8d), both these shells have reached the center of the fiber, so all boron has been consumed. The slower MgB_2 shell continues its radial growth, while the MgB_2 wedges thicken and merge with each other, leaving shrinking MgB_4 slivers in regions far from cracks.

We consider here a simplified model consisting of a MgB_2 shell together with N MgB_2 wedges defined by N cracks which are equally distributed along the circumference of the fiber. Each wedge eventually fills a sector with angle $2\alpha = 2\pi/N$ in the fiber cross-section. The model is two-dimensional, since the fibers are assumed to be cylindrical in shape. As illustrated in Fig. 9a, it is sufficient to model half the sector with angle $\alpha = \pi/N$, which contains two growing MgB_2 regions: (i) a MgB_2 shell with area A_s, and (ii) a MgB_2 half-wedge with area A_w. Mg diffusion is shown schematically in Fig. 9a to occur radially through the MgB_2 shell and circumferentially through the half-wedge, assuming that Mg fills at all times a radial crack at the center of the wedge, assumed to be of negligible thickness. The total MgB_2 area A_{tot} in the half-sector (and thus the total MgB_2 volume in the fiber, given the cylindrical shape of the fibers and the assumption that wedges are equidistant) is taken as the sum of the shell area A_s and the area of the half-wedge A_{wf} in the MgB_4 shell ahead of the MgB_2 shell. The model does not capture the complex shape expected to exist at the MgB_2/MgB_4 interface in the regions where the shell and the wedge intersect.

First, the shell area A_s that would exist in the absence of the wedge and is growing radially into the cylindrical fiber is

$$A_S = \frac{z}{2N}\left(\pi r_0^2 - \pi(r_0 - h')^2\right), \tag{4}$$

where h', defined above, is calculated from Eq. (3) with D_{MgB_2} valid from 0 to r_0. The half-wedge area A_w, that would be created in the absence of the shell, is growing in two directions. First, its height c (corresponding to the crack length extending to the MgB_4/MgB_7 shell interface) increases with the diffusion-controlled radial growth of that interface determined from Eq. (3) with D_{MgB_4} (valid to the maximum value of r_0). Second, the half-length b of the chord increases by the diffusion-controlled circumferential growth of MgB_2 perpendicularly to the crack, which is determined from Eq. (3) with D_{MgB_2}. The half-wedge area

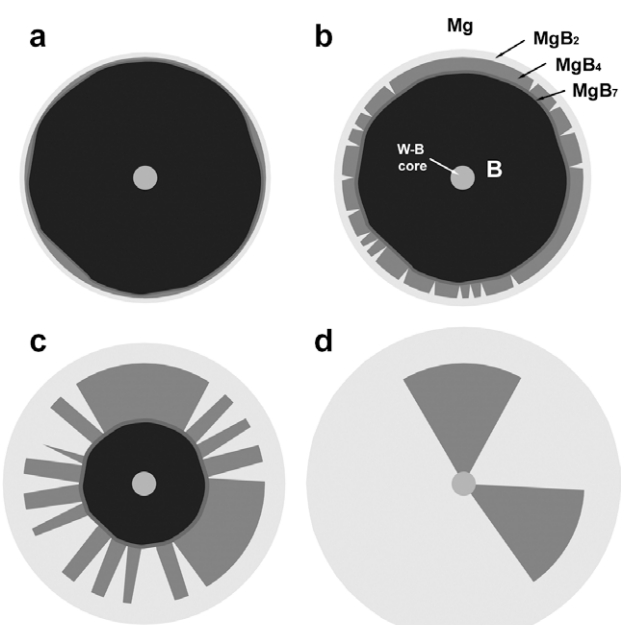

Fig. 8. Schematic illustrating simplified fiber reaction process. (a) Cylindrical shells of MgB_7, MgB_4, and MgB_2 grow radially into B fiber; (b) continuing radial growth is accompanied by cracks in the MgB_4 shell due to misfit stresses; these cracks fill with reaction product, forming MgB_2 wedges; (c) MgB_2 cracks and associated wedges extend radially as the MgB_4 shell penetrates into the fiber, and wedges grow circumferentially by reaction with the surrounding MgB_4; (d) MgB_4 shell and associated MgB_2 wedges reach the W–B fiber core, and MgB_2 wedges thicken and merge, leaving in some areas unreacted MgB_4 slivers (two are shown in schematic) which eventually disappear by circumferential growth of the MgB_2 wedges and radial growth of the MgB_2 shell.

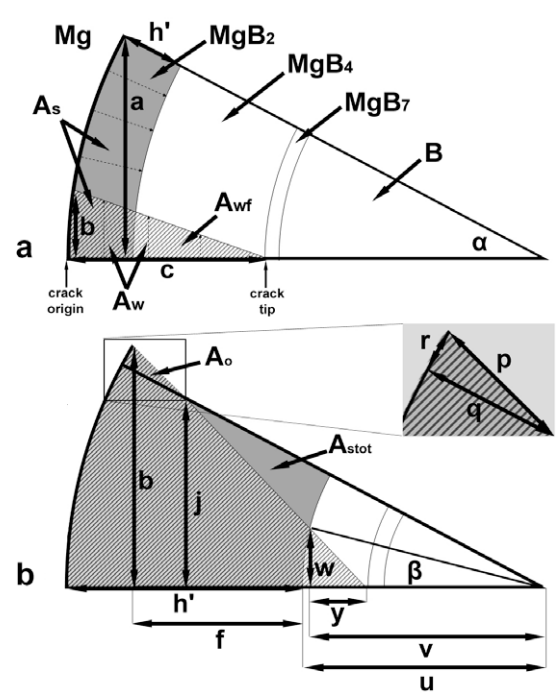

Fig. 9. (a) Schematic showing the half sector of fiber with grey MgB_2 regions used in simplified model. The MgB_2 region consists of a shell with area A_s growing radially by diffusion of Mg from fiber surface, and a MgB_2 half-wedge with area A_w with crack length c determined by the radial growth of the MgB_4 phase front into the fiber and half-length b determined by the circumferential growth of MgB_2 perpendicularly to the crack. (b) Schematic showing fiber at a later time during reaction, when the calculated half-wedge extends beyond the fiber half sector area by A_o.

A_w is determined from the two above parameters, b and c, as

$$A_w = \frac{z}{2}\left[fb + \frac{1}{2}r_0^2\left(2\sin^{-1}\left(\frac{b}{r_0}\right) - \sin\left(2\sin^{-1}\left(\frac{b}{r_0}\right)\right)\right)\right], \tag{5}$$

where b, c and f (itself a function of r_0, b and c) are given in Appendix B. The above equation does not prevent the half-wedge from growing beyond its particular fiber half-sector, which is unphysical since it would produce overlap with a neighboring half-wedge. The overlap area A_o, shown in Fig. 9b, is given as

$$A_o = z(s(s-r)(s-p)(s-q))^{1/2} + \frac{zr_0^2}{2}\left(2\sin^{-1}\left(\frac{r}{2r_0}\right) - \sin\left(2\sin^{-1}\left(\frac{r}{2r_0}\right)\right)\right), \tag{6}$$

where the parameters p, q, r and s are given in Appendix B. Additionally, the section of the half-wedge, A_{wf}, that is in front of the reacted shell is calculated as

$$A_{wf} = \frac{z}{2}\left[wy + \frac{1}{2}u^2\left(2\sin^{-1}\left(\frac{w}{u}\right) - \sin\left(2\sin^{-1}\left(\frac{w}{u}\right)\right)\right)\right], \tag{7}$$

where the parameters u, w and y are given in Appendix B.

The shell contribution to the total reaction, A_{stot}, which is not associated with the half-wedge A_w is determined as

$$A_{stot} = A_s - (A_w - A_{wf} - A_o) \tag{8}$$

for $\beta < \alpha$ (with β shown in Fig. 9b). The half-wedge contribution to the total reaction, A_{wtot}, is calculated as

$$A_{wtot} = A_w - A_o. \tag{9}$$

The total reacted area, A_{tot}, is then found by adding the half-wedge and shell contributions given by Eqs. (8) and (9):

$$A_{tot} = A_s + A_{wf}, \tag{10}$$

which is a simplified view not taking into account the complex diffusion field near the region where shell and half-wedge overlap. The degree of reaction x is finally calculated as

$$x = A_{tot}/A_{sect}, \tag{11}$$

where $A_{sect} = z\alpha r_0^2$ is the area of the fiber half sector after complete reaction. Introducing into Eq. (11) the two area equations (Eqs. (4) and (7)) and the equations for the geometrical parameters (u, w and y given in the Appendix) provides a bulky close-form analytical solution for the degree of reaction x as a function of the reaction time t with the following parameters: one geometrical parameter (the initial fiber radius r_0), two diffusion coefficients (D_{MgB_2} and D_{MgB_4}, themselves dependent on temperature), and two reaction parameters (the volume expansion coefficient z and the number of cracks N). Of these, only N is not known a priori.

4.4. Model predictions and comparison to data

Model predictions for the degree of reaction as a function of reaction time are shown in Fig. 10a and b for 7 or 30 cracks per fiber, using the MgB_2 and MgB_4 diffusion coefficients at 900 °C determined in the previous sections. In this figure, the combined contributions of the shell and wedges (Eq. (11)) are shown, as well as the contributions of the shell without wedges (A_s given in Eq. (4)) and the wedges without shells (A_w–A_0, from Eqs. (5) and (6)). These single wedge or shell contributions are hypothetical, since shell and wedges always coexist, but they illustrate the relative importance of each mechanism.

With $N = 30$ at 900 °C (Fig. 10a), the reaction is completed after ~11 h. MgB_2 wedge growth, occurring simulta-

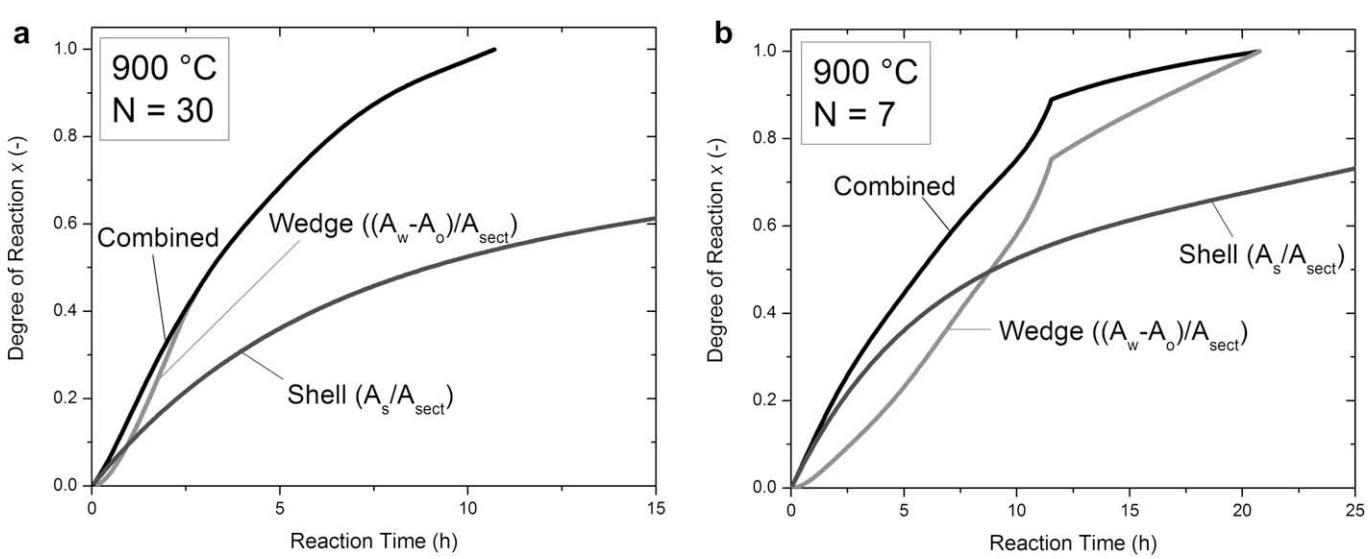

Fig. 10. Model predictions for degree of MgB_2 reaction as a function of time, showing the combined contributions of the shell and wedges (A_{tot}/A_{sect}, Eq. (10), as well as two extreme cases where MgB_2 growth occur only through the shell without wedges (A_s/A_{sect}, Eq. (4)) and only through wedges without the shell ($(A_w - A_0)/A_{sect}$, Eqs. (5) and (6)). Plots are given for (a) a high crack number ($N = 30$) and (b) a low crack number ($N = 7$).

neously in the radial and circumferential directions, is controlling the reaction rate, while the MgB_2 shell contributes only early in the reaction. With $N = 7$ (Fig. 10b), the reaction proceeds more slowly, and shows an inflection point after ~90% completion. This inflection corresponds to the time when the MgB_2 wedges reach the center of the fiber, so that further wedge growth occurs only laterally. Radial shell growth contributes significantly throughout the reaction. This situation is observed in the micrograph shown in Fig. 3b with MgB_2 wedges having reached the W–B core of the fiber even though the degree or reaction is only 40%. In both cases (Fig. 10a and b), the time to complete the reaction would be much longer if wedges were not present.

As shown in Fig. 11a and b for 900 and 1000 °C, increasing the number of cracks improves reaction kinetics, since the diffusion distances for circumferential MgB_2 wedge growth are reduced. It is apparent that, for $N > 15$, the reaction time does not decrease significantly, as it is dictated mostly by the radial growth of the MgB_2 wedge height, which is itself given by the growth of the MgB_4 shell.

The diffusion coefficients for MgB_2 and MgB_4 calculated above (Fig. 7a and b) have sizeable error bars as expressed by errors on their activation energies ($Q = 362 \pm 41$ and 477 ± 41 kJ mol^{-1}, respectively). To assess the effect of these uncertainties, calculations were performed using the upper and lower bounds as well as the average value of the diffusion coefficients at 900 °C; the results are plotted in Fig. 12a and b for two crack numbers ($N = 5$ and 30). The slope of the quasi-linear region for $x = 0$–0.6 varies by a factor 2–3 when using the extreme values of the diffusion coefficients. Similarly, the average time to reach full reaction ($x = 1$) is 35 h for $N = 5$, with a lower and upper bounds of 24 and 62 h (Fig. 12b); for $N = 30$, the average time is 11 h, and varies from 6 to 25 h (Fig. 12a). These are probably extreme cases, since both diffusion coefficients D_{MgB_2} and D_{MgB_4} are taken to their limits given by the error bars of the activation energies.

The effects of errors for each diffusion coefficient at 900 °C are isolated and compared in Fig. 13a and b for $N = 5$ and 30, where D_{MgB_2} is varied while maintaining D_{MgB_4} constant, and in Fig. 13c and d, where the inverse situation is examined. It is apparent that D_{MgB_2} controls the reaction time when the number of cracks is low ($N = 5$, Fig. 13a and c) while D_{MgB_4} controls reaction time when it is high ($N = 30$, Fig. 13b and d). This is because the overall reaction rate is a function of both the MgB_2 wedge length (controlled by D_{MgB_4}) and the MgB_2 wedge width and MgB_2 shell depth (both controlled by D_{MgB_2}). Thus, D_{MgB_4} affects most the initial reaction rate while D_{MgB_2} controls the final reaction rate after wedges reach the fiber center. Since, for a large number of cracks, the wedges reach the fiber center only near the end of the reaction, D_{MgB_4} controls the total reaction time, as illustrated in Fig. 13b and d.

The curves for degree of reaction measured in situ by diffraction as a function of reaction time, shown in Fig. 1 for reaction temperatures of 885–1025 °C, can then be modeled based on the measured diffusion coefficients for MgB_2 and MgB_4, and the average number of cracks per fiber N. Adjusting values for these three parameters within the relatively small window given by experimental observations (i.e. error bars for the diffusion coefficients and metallographic observation for N), fits to the experimental curves are shown in Fig. 14a–c for 900, 950 and 1000 °C, spanning the temperature range studied here (885–1025 °C). At 900 °C (Fig. 14a), a good fit is obtained for $D_{MgB_2} = 10^{-13}$ m^2 s^{-1}, $D_{MgB_4} = 10^{-12}$ m^2 s^{-1}, and $N = 8$. At 950 °C (Fig. 14b), these values are $D_{MgB_2} = 7 \times 10^{-13}$ m^2 s^{-1}, $D_{MgB_4} = 7 \times 10^{-12}$ m^2 s^{-1}, and $N = 7$; at 1000 °C, they are $D_{MgB_2} = 15 \times 10^{-13}$ m^2 s^{-1}, $D_{MgB_4} = 16 \times 10^{-12}$ m^2 s^{-1}, and $N = 4$ (Fig. 14c). The fits are further improved if the curves are

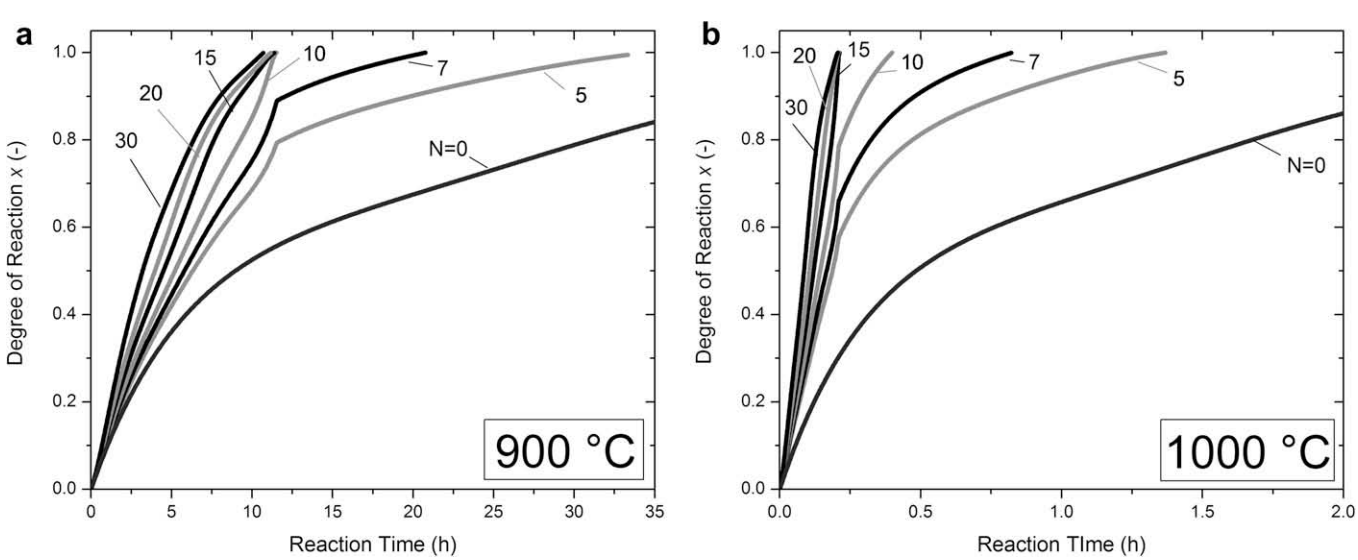

Fig. 11. Model predictions for degree of MgB_2 reaction as a function of time for various crack numbers N at (a) 900 °C and (b) 1000 °C.

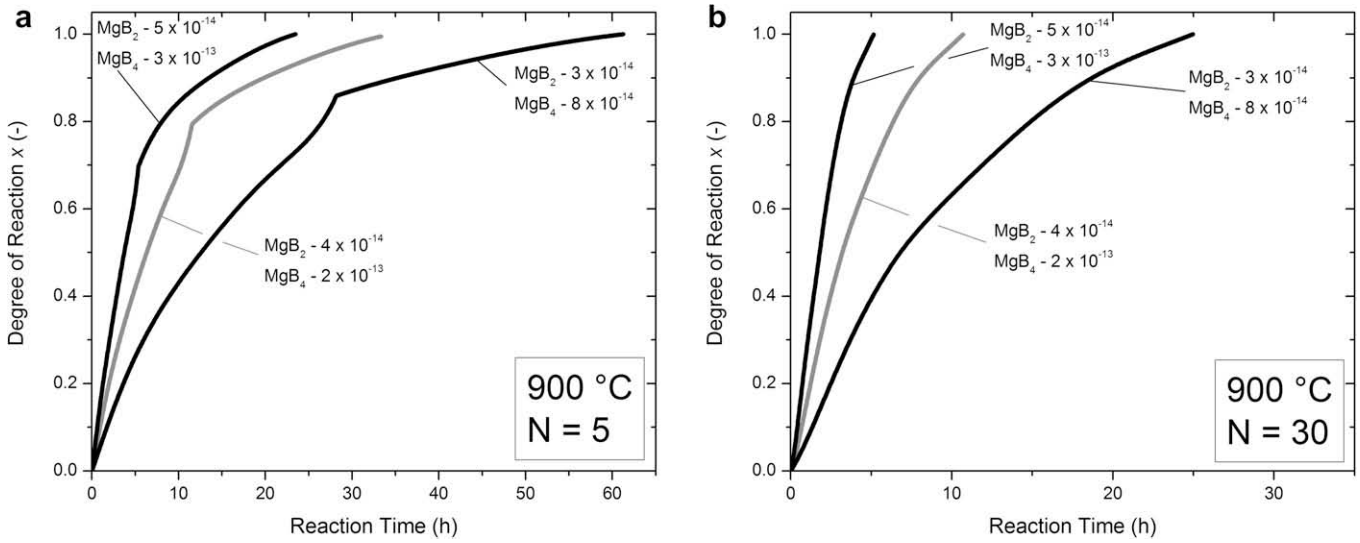

Fig. 12. Model predictions for degree of MgB_2 reaction as a function of time at 900 °C, for upper and lower bounds as well as average values of the MgB_2 and MgB_4 diffusion coefficients, for (a) a low crack number ($N = 5$), and (b) a high crack number ($N = 30$).

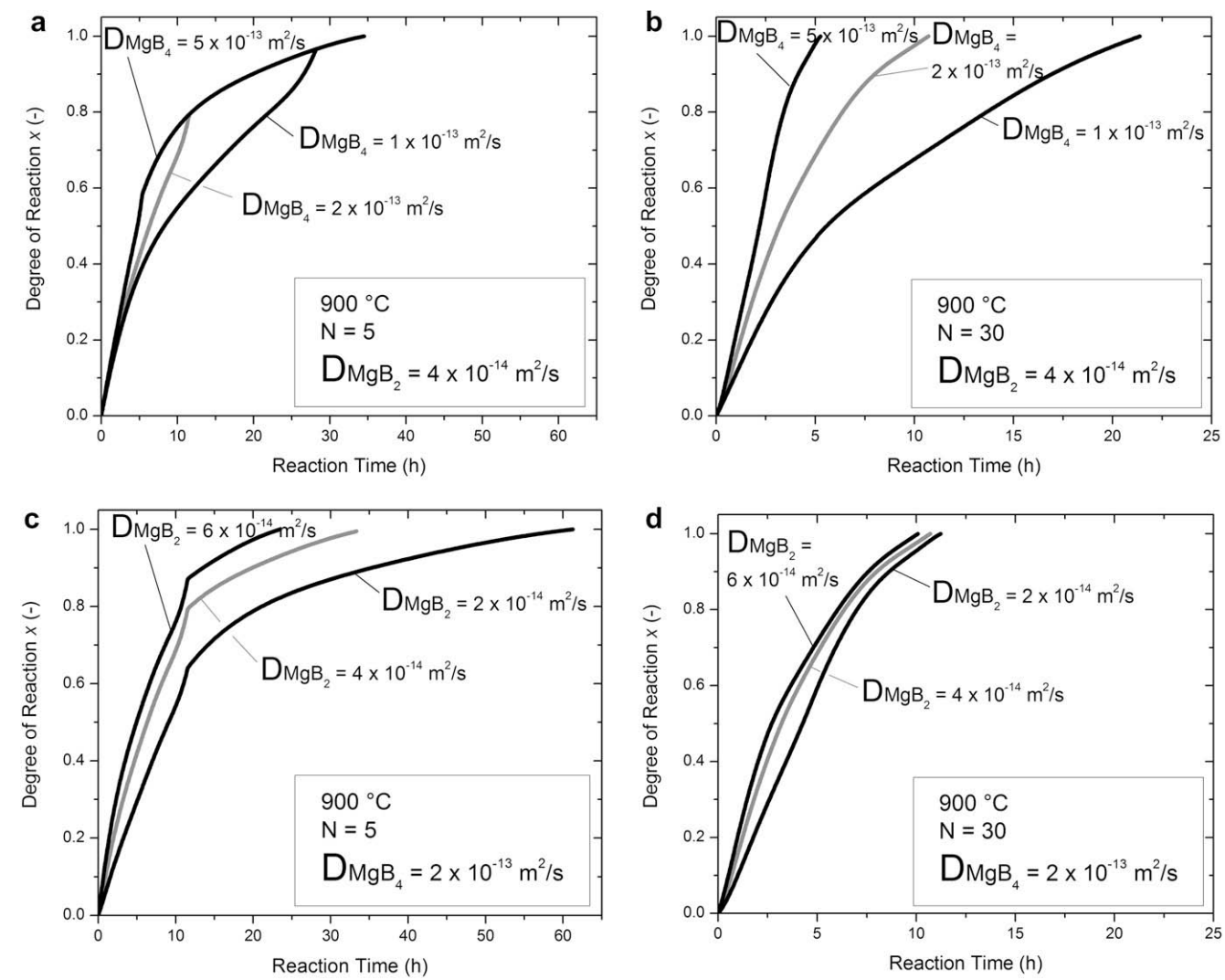

Fig. 13. Model predictions for degree of MgB_2 reaction as a function of reaction time at 900 °C for two crack numbers ($N = 5$ and 30): (a and b) with D_{MgB_2} varied within its error range and D_{MgB_4} constant; (c and d) with D_{MgB4} varied within its error range and D_{MgB_2} constant.

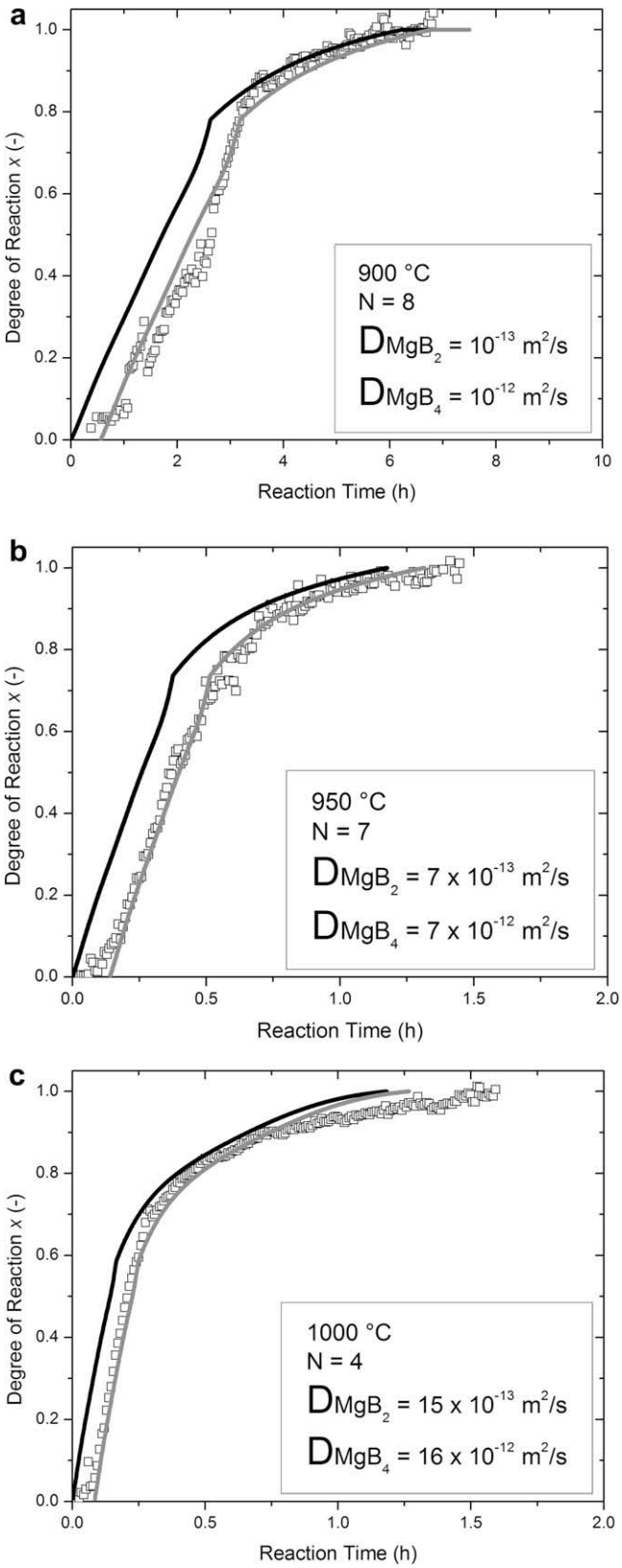

Fig. 14. Model predictions for degree of MgB_2 reaction as a function of reaction time at (a) 900 °C; (b) 950 °C; (c) 1000 °C compared to experimental data from Fig. 1. Fitted values for crack number and MgB_2 and MgB_4 diffusion coefficients are given in figures. Dark lines correspond to the model, and light lines are shifted by a fitted incubation time.

shifted by 2000, 500 and 300 s, respectively, to take into account the incubation time of the reaction. At 900 and 1000 °C, good fits necessitate diffusion coefficients greater than experimentally measured by ex situ studies (Fig. 7), reaching the upper limit of the error bars at 1000 °C and exceeding by nearly an order of magnitude the average value at 900 °C. Additionally, these fits used only four to eight cracks, whereas metallographic observation reveals 20–30 cracks in the early stages of fiber reaction at 900 and 1000 °C (Fig. 2). At later stages, however, the number of wedges decreases as illustrated in Fig. 3b, most probably as a result of wedge merging as shown schematically in Fig. 8.

To improve the model, the number of cracks could be time-dependent, increasing (due to nucleation of new cracks) or decreasing (due to merging of closely spaced cracks) with increasing reaction time. Also, an assembly of fibers could be modeled, with a distribution of crack time-dependent numbers, spatial distribution and incubation times. The current simplified model captures the main physical aspects of the reaction, so these or other refinements are not explored here, especially in view of the considerable experimental errors associated with the diffusion coefficients and the difficulty in determining the number of cracks a priori.

5. Conclusions

Boron fibers with 140 μm diameter were reacted with excess liquid Mg to form MgB_2 fibers within a Mg matrix. Metallographic ex situ examination of fibers, partially reacted between 700 and 1000 °C, shows that reaction occurs by two concurrent mechanisms: (i) the radial growth of cylindrical MgB_2, MgB_4 and MgB_7 shells; and (ii) the radial and circumferential growth of MgB_2 wedges initiated by radial cracks of the MgB_4 or MgB_7 shells.

MgB_2 formed by the first mechanism is modeled by considering diffusion-controlled growth of a cylindrical reaction front, leading to reaction rates for MgB_2 as well as effective diffusion coefficients for MgB_2, MgB_4 and MgB_7 spanning from $3 \times 10^{-17}\,m^2\,s$ at 700 °C to $1 \times 10^{-11}\,m^2\,s^{-1}$ at 1000 °C, with activation energies of 360, 480 and 320 kJ mol^{-1}, respectively.

MgB_2 formation by the second mechanism is controlled by the radial growth of the wedges (given by the diffusion-controlled growth of the MgB_4 or MgB_7 shells) and by the circumferential thickening of the wedges, controlled by the MgB_2 diffusion coefficient.

The two contributions – from MgB_2 shell and wedges – are combined in a simplified analytical model which predicts the conversion of B fibers to MgB_2 as a function of time, diffusion coefficients, fiber radius and crack number. Using physically reasonable values for these parameters, model predictions are in good agreement with experimental data for degree of reaction as a function of time, measured in situ between 885 and 1025 °C by synchrotron X-ray diffraction.

Acknowledgments

This work was supported by the US National Science Foundation through Grant No. DMR-0319051. The authors thank Dr. J. Marzik of Specialty Materials, Inc. for providing boron fibers and Drs. J. Quintana, Q. Ma and D. Keane for help in performing the diffraction experiments at the DuPont-Northwestern-Dow Collaborative Access Team (DND-CAT). DND-CAT is supported by E.I. DuPont de Nemours & Co., The Dow Chemical Company and the State of Illinois and is located at Sector 5 of the Advanced Photon Source which is supported by the US Department of Energy under Contract No. DE-AC02-06CH11357.

Appendix A

Carter [18] gives an derivation for the rate constants k of a spherical powder reacting into a single product. This derivation is adapted here to the case of a cylindrical fiber. At any time during the reaction, the volume Q_B of unreacted boron is

$$Q_B = \pi r_1^2 L, \tag{A1}$$

where r_1 is the radius of the unreacted fiber cylinder and L is the fiber length. The rate of change of the amount of unreacted B for a cylinder is given by Crank [22] as

$$\frac{dQ_B}{dt} = \frac{-2\pi k L}{\ln\left(\frac{r_2}{r_1}\right)}, \tag{A2}$$

where k is the reaction rate constant and r_2 is the overall radius of the partially reacted fiber. Differentiating Eq. (A1) with time and setting equal to Eq. (A2), results in

$$r_1 \frac{dr_1}{dt} = \frac{-k}{\ln\left(\frac{r_2}{r_1}\right)}. \tag{A3}$$

This equation can be rewritten as

$$-k dt = r_1 \ln\left(\frac{\sqrt{z r_0^2 + (1-z) r_1^2}}{r_1}\right) dr_1, \tag{A4}$$

after introducing into Eq. (A3) the following mass conservation equation:

$$r_2 = \sqrt{z r_0^2 + r_1^2 (1-z)}, \tag{A5}$$

where r_0 is the initial radius of the cylindrical fiber before reaction and z is the volume expansion coefficient upon reaction. Integrating both sides of Eq. (A4) and substituting $r_1^2 = (1-x) r_0^2$ provides the following equation (labeled Eq. (2) in the main text), relating the reaction rate constant k to the degree of reaction x:

$$-kt = \frac{r_0^2\left(x \ln\left(\frac{1-x+zx}{1-x}\right) + zx \ln\left(\frac{1-x}{1-x+zx}\right) + z \ln\left(\frac{1}{1-x}\right) + \ln\left(\frac{1-x}{1-x+zx}\right)\right)}{4(z-1)}. \tag{A6}$$

Additionally, the degree of reaction x can be expressed from geometrical considerations as a function of $h = r_2 - r_1$, which is the thickness of the reaction product shell on the cylindrical unreacted inner region. Substituting Eq. (A5) and $r_1^2 = (1-x) r_0^2$ into Eq. (A6) and rearranging results in a quadratic equation:

$$2 h r_0 \sqrt{1-x} - z x r_0^2 + h^2 = 0, \tag{A7}$$

which can be solved for x and rearranged into:

$$x = \left(\frac{h}{z r_0}\right)^2 \left(z - 2 + 2\sqrt{1 - z + (z r_0/h)^2}\right). \tag{A8}$$

Appendix B

The various geometrical parameters associated with the half-wedge areas (Eqs. (5)–(7)) are shown in Fig. 9 and are determined from geometrical considerations as

$$a = r_0 \sin\alpha \tag{B1}$$

$$f = \sqrt{r_0^2 - b^2} - r_0 + c \tag{B2}$$

$$j = \frac{-(r_0 - c) a b}{-b r_0 + b\left(r_0 - \sqrt{r_0^2 - a^2}\right) + f a} \tag{B3}$$

$$p = \sqrt{b^2 + f^2} - \frac{j\sqrt{b^2 + f^2}}{b} \tag{B4}$$

$$q = r_0 - \frac{j r_0}{a} \tag{B5}$$

$$r = \sqrt{(b-a)^2 + \left(c - f - r_0 + \sqrt{r_0^2 - a^2}\right)^2} \tag{B6}$$

$$s = \frac{1}{2}(p + q + r) \tag{B7}$$

$$u = r_0 - h' \tag{B8}$$

$$v = \frac{1}{(b^2 + f^2)}\left[b^2 (r_0 - c) + \sqrt{b^2 f^2 u^2 - f^2 b^2 (r_0 - c)^2 + f^4 u^2}\right] \tag{B9}$$

$$w = \sqrt{u^2 - v^2} \tag{B10}$$

$$y = v - r_0 + c \tag{B11}$$

$$\beta = \sin^{-1}\left(\frac{w}{u}\right) \tag{B12}$$

References

[1] Baranov AN, Solozhenko VL, Lathe C, Turkevich VZ, Park YW. Superconductor Science and Technology 2003;16:1147.
[2] DeFouw JD, Quintana JP, Dunand DC. Acta Materialia 2008;56:1680.
[3] Grivel JC, Pinholt R, Andersen NH, Kovac P, Husek I, Homeyer J. Superconductor Science and Technology 2006;19:96.
[4] Yan SC, Lu YF, Liu GQ, Yan G, Zhou L. Journal of Alloys and Compounds 2007;443:161.
[5] Glowacki BA, Majoros M, Vickers M, Evetts JE, Shi Y, McDougall I. Superconductor Science and Technology 2001;14:193.
[6] Kumakura H, Kitaguchi H, Matsumoto A, Hatakeyama H. Applied Physics Letters 2004;84:3669.
[7] Fang H, Padmanabhan S, Zhou YX, Salama K. Applied Physics Letters 2003;82:4113.

[8] Soltanian S, Wang XL, Kusevic I, Babic E, Li AH, Qin MJ, et al. Physica C 2001;361:84.
[9] Goldacker W, Schlachter SI, Obst B, Eisterer M. Superconductor Science and Technology 2004;17:S490.
[10] Canfield PC, Finnemore DK, Bud'ko SL, Ostenson JE, Lapertot G, Cunningham CE, et al. Physical Review Letters 2001;86:2423.
[11] DeFouw JD, Dunand DC. Applied Physics Letters 2003;83:120.
[12] Chawla KK. Fibrous Materials. Cambridge and New York: Cambridge University Press; 1998.
[13] Dunand DC. Applied Physics Letters 2001;79:4186.
[14] Hammersley AP, Svensson SO, Hanfland M, Fitch AN, Hausermann D. High Pressure Research 1996;14:235.
[15] Finnemore DK, Straszheim WE, Bud'ko SL, Canfield PC, Anderson NE, Suplinskas RJ. Physica C-Superconductivity and its Applications 2003;385:278.
[16] Wilke RHT, Bud'ko SL, Canfield PC, Finnemore DK, Suplinskas RJ, Hannahs ST. Physica C-Superconductivity and Its Applications 2005;424:1.
[17] Balducci G, Brutti S, Ciccioli A, Gigli G, Manfrinetti P, Palenzona A, et al. Journal of Physics and Chemistry of Solids 2005;66:292.
[18] Carter RE. Journal of Chemical Physics 1961;34:2010.
[19] Young ML, DeFouw J, Almer JD, Dunand DC. Acta Materialia 2007;55:3467.
[20] Kim HM, Yim SS, Kim KB, Moon SH, Kim YW, Kang DH. Journal of Materials Research 2004;19:3081.
[21] Entchev PB, Lagoudas DC, Slattery JC. International Journal of Engineering Science 2001;39:695.
[22] Crank J. The Mathematics of Diffusion. Oxford: Clarendon Press; 1975.